

Tracking the photodissociation probability of D_2^+ induced by linearly chirped laser pulses

András Csehi,¹ Gábor J. Halász,² Lorenz S. Cederbaum,³ and Ágnes Vibók^{1,4}

¹*Department of Theoretical Physics, University of Debrecen,
H-4010 Debrecen, PO Box 5, Hungary*

²*Department of Information Technology,
University of Debrecen, H-4010 Debrecen, PO Box 12, Hungary*

³*Theoretische Chemie, Physikalisch-Chemisches Institut,
Universität Heidelberg, H-69120 Heidelberg, Germany*

⁴*ELI-ALPS, ELI-HU Non-Profit Ltd,
H-6720 Szeged, Dugonics tér 13, Hungary*

Abstract

In the presence of linearly varying frequency chirped laser pulses the photodissociation dynamics of D_2^+ is studied theoretically after ionization of D_2 . As a completion of our recent work (J. Chem. Phys. **143**, 014305 (2015)) a comprehensive dependence on the pulse duration and delay time is presented in terms of total dissociation probabilities. Our numerical analysis carried out in the recently introduced light-induced conical intersection (LICI) framework clearly shows the effects of the changing position of the LICI which is induced by the frequency modulation of the chirped laser pulses. This impact is presented for positively, negatively and zero chirped short pulses.

I. INTRODUCTION

The dynamics initiated in a molecule by photon impact is usually described using the Born-Oppenheimer (BO) approximation [1], where the fast electrons are treated separately from the slow nuclei. In this picture, electrons and nuclei do not easily exchange energy. However, at some nuclear configurations, in particular, in the vicinity of degeneracy points or conical intersections (CIs) this energy exchange may become important [2–9]. It is widely accepted today that conical intersections are fundamental in the nonadiabatic processes which are ubiquitous in photophysics and photochemistry [10–12]. At these CIs, a molecule can switch efficiently between two different energy surfaces on a time scale faster than a single molecular vibration. CIs are associated with phenomena like dissociation, radiationless relaxation of excited states, proton transfer, etc., and are also important in biological molecules [13–15].

For diatomic molecules that have only one degree of freedom, it is not possible for two electronic states of the same symmetry to become degenerate and as a consequence of the well-known noncrossing rule an avoided crossing results. However, it is the situation only in free space. It was presented in previous papers that conical intersections can be created in a molecular system both by running and standing laser waves even in diatomics [16, 17]. In this case the laser light couples either the center of the mass motion with the internal rovibrational degrees of freedom (in case of standing laser field) or the vibrational motion with the emerged rotational degree of freedom (in the case of running laser field) and the so-called light-induced conical intersection (LICI) arises. By varying the laser parameters (intensity and frequency), it is possible to affect the position and structure of the LICIs, and thus control the dynamics in order to study how molecules behave near a light-induced CI. An interesting framework to understand this dynamics draws parallel with conical intersections (CIs) between electronic surfaces in polyatomic molecules.

A few years ago, we started a systematic study of the nonadiabatic effects induced by laser waves in molecular systems. It has been demonstrated along with other groups that LICIs have a significant impact on several different dynamical properties (like molecular spectra, molecular alignment, fragment angular distribution, branching ratio etc.) of both diatomic [18–23] and polyatomic molecules [24–30]. Recently we have made particular efforts for

understanding the photodissociation process of such a simple system as the D_2^+ in the LICI framework [31–36]. The dissociation of D_2^+ and its isotopologue, H_2^+ have been extensively studied in the last couple of decades [37–67]. We note here that the effect of frequency chirped laser pulses on the dissociation dynamics have been thoroughly investigated in the last fifteen years [68–78]. Several different dynamical properties like kinetic energy release spectra, total dissociation probabilities as well as angular distributions have been studied.

In our latest work [35] we used linearly chirped laser pulses for initiating the dissociation dynamics of D_2^+ . In contrast to the constant frequency (transform limited, TL) laser fields, chirped pulses give rise to LICIs with a varying position according to the temporal frequency change. In that work an interesting phenomenon was revealed but the explanation remained unclear. Namely, it was found that the amplitude of the periodic change in the dissociation probability as a function of delay time is significantly compressed by the chirped pulse compared to the transform limited situation.

The present investigation is a natural extension of our previous work and now we provide a clear explanation for the origin of the physical phenomena beyond the enhanced and suppressed dissociation processes induced by chirped laser pulses. For that purpose, numerical simulations are performed using different laser pulses. A full dimensional (2D) scheme was applied to the problem in which the rotational angle is assumed as a dynamic variable and, therefore, the LICI is explicitly taken into account.

The article is arranged as follows. In the next two sections, we present the methods and algorithms required for the theoretical study. The calculated dynamical quantities and the numerical details are also briefly summarized there. In the fourth section, we present and discuss the numerical results for the D_2^+ system. In the last section conclusions and future plans will be given.

II. THE D_2^+ MOLECULE

This section is devoted to the description of the most relevant features of the system under investigation. The reason for choosing D_2^+ for the numerical analysis lies in its simplicity: (i) by having only one electron in the system, electron correlation effects do not play a role and (ii) by being a diatomic molecule there is only one internal nuclear degree of freedom. All these properties make possible the accurate treatment of D_2^+ from the theoretical point of view. Furthermore the above simple properties allow us to purely focus on physical aspects by excluding possible disturbing factors.

In our treatment the ground and first excited electronic states of D_2^+ molecular ion ($V_1 = 1s\sigma_g$ and $V_2 = 2p\sigma_u$) are considered (see in Fig. 1). After a sudden ionization of the neutral D_2 at $t = 0$, its vibrational ground state is vertically transferred to $V_1 = 1s\sigma_g$ and is considered as the initial wave packet in our simulations. The vibrational wave packet created in this manner is not in an energetic eigenstate of the V_1 diabatic potential, it can be regarded as the superposition or Franck Condon distribution of the vibrational eigenstates of D_2^+ .

After ionization, the $V_1(R)$ and the repulsive $V_2(R)$ electronic states are radiatively coupled by the laser field and light-induced electronic transition occurs due to the non-zero transition dipole moment $d(R)$ related to the electronic states:

$$d(R) = -\langle \xi_1^{el} | \sum_k r_k | \xi_2^{el} \rangle. \quad (2.1)$$

In the space of the $V_1(R)$ and $V_2(R)$ electronic states the time-dependent nuclear Hamiltonian including the ro-vibronic motion and the light-matter coupling reads as follows (using atomic units i.e. $e=m_e=\hbar=1$):

$$H_{nuc} = \left(-\frac{1}{2\mu} \frac{\partial^2}{\partial R^2} + \frac{L_{\theta\phi}^2}{2\mu R^2} \right) \mathbf{1} + \begin{pmatrix} V_1(R) & -\epsilon(t)d(R)\cos\theta \\ -\epsilon(t)d(R)\cos\theta & V_2(R) \end{pmatrix}. \quad (2.2)$$

Here R and (θ, ϕ) are the vibrational and rotational coordinates, respectively. θ is associated with the angle between the molecular axis and the laser polarization direction and the ϕ -dependence is not present in our simulations as the initial wave packet is in its rotational

ground state ($J = 0$). $L_{\theta\phi}$ denotes the angular momentum operator of the nuclei, μ is the reduced mass and $\epsilon(t)$ is the electric field.

The potential energy and the dipole moment functions were taken from Refs. [79] and [80]. The actual form of the applied $\epsilon(t)$ electric field will be detailed in the next section.

After having all the necessary parameters of the system we are able to carry out the nuclear dynamical simulations using the full time-dependent Hamiltonian in (2.2). A very useful pictorial tool for understanding the laser-matter interaction processes, especially in the strong field physics is the so called Floquet representation of the nuclear Hamiltonian [18, 21, 81]. In our presentation we use this time-independent scheme only for the illustration of the LICI phenomenon. In this picture the $V_2(R)$ potential energy curve is shifted downwards by $\hbar\omega_0$ upon interaction with a laser field of ω_0 frequency. As a result of it a crossing is formed between the diabatic ground and the dressed excited potential energy curves (Fig.1). After diagonalizing the diabatic potential matrix in (2.2), the resulting adiabatic or light-induced surfaces (V_l and V_u in Fig. 1) form a conical intersection for geometry parameters determined by the following conditions [16, 17]:

$$\cos\theta = 0 \quad (\theta = \frac{\pi}{2}) \quad \text{and} \quad V_1(R) = V_2(R) - \hbar\omega_0. \quad (2.3)$$

An important feature of the created light-induced conical intersections as compared to the natural CIs is that their fundamental characteristics can be modified by the external field. It has already been shown that the intensity of the field determines the strength of the nonadiabatic coupling, namely the steepness of the cone, while the energy of the field specifies the position of the LICI. Therefore by applying chirped or frequency modulated laser pulses the position of the LICI is continuously changing during the dynamical process making possible in principle, monitoring the time evolving nuclear wave packet, by properly chosen chirp and laser parameters.

III. COMPUTATIONAL DETAILS

In our numerical analysis carried out for D_2^+ the focus was on the calculation of dissociation probabilities resulting from the application of different external laser fields. This quantity was derived according to the following formula [85]:

$$P_{diss} = \int_0^{\infty} dt \langle \psi(t) | W | \psi(t) \rangle \quad (3.1)$$

where $-iW$ is the complex absorbing potential (CAP) applied at the last 10 *a.u.* of the vibrational (*R*) grid.

The vibrational ground state of D₂ was taken as the initial wave packet ($t < 0$ *fs*) for D₂⁺ furthermore the molecule was initially in its rotational ground state ($J = 0$) in our calculations. Linearly polarized Gaussian laser pulses were applied for initiating the dissociation process. The dissociation probabilities were calculated as a function of the delay time of the pulse with respect to the sudden ionization ($t = 0$ *fs*). This delay time was described by the t_{delay} parameter (the temporal maximum position of the field) which was ranging from 0 to 80 *fs*.

The central wavelength of the field was $\lambda_0 = 200$ *nm* ($\hbar\omega_0 = 6.199$ *eV*) and due to the chirping effect the frequency was changing linearly around t_{delay} . The frequency changing rate depends on the chirp parameter which is closely related to the pulse duration (as will be detailed in the next section). In order to be able to follow the nuclear motion we always tried to achieve proper chirp values. Accordingly, maximum possible values had to be considered, namely for 1 *fs* and 2 *fs* short pulses the chirp parameters were $a = \pm 0.3$ and $a = \pm 0.15$, respectively, while in [35] for longer ($T_p = 10$ *fs*) pulses $a = \pm 0.03$ were adopted.

Relatively large intensity (10^{13} *W/cm*²) had to be utilized so as to maximize the effect of the created LICl. Numerical simulations will be presented with positively and negatively chirped as well as transform limited (TL) laser pulses.

A. The electric field

Linearly polarized Gaussian laser pulses with linearly varying frequencies have been applied during our time propagations. The electric field is defined as the time derivative of the Gaussian shaped vector potential:

$$\epsilon(t) = -\frac{\partial}{\partial t} A(t) \quad (3.1.1)$$

where the $A(t)$ vector potential has the following form:

$$A(t) = \frac{-\epsilon_0}{\sqrt[4]{1 + \beta^2}} \cdot \sin \left\{ \omega_0(t - t_{delay}) - \frac{\alpha}{2}(t - t_{delay})^2 + \varphi_0 \right\} \cdot e^{-\frac{2 \log 2}{1 + \beta^2} \left(\frac{t - t_{delay}}{T_p} \right)^2}. \quad (3.1.2)$$

In the above expression ϵ_0 is the maximum field amplitude, ω_0 is the carrier frequency, while T_p and t_{delay} are the TL pulse duration (at FWHM) and the temporal maximum of the pulse, respectively. In (3.1.2) φ_0 is the carrier envelope phase (CEP, zero in the present study), α and β are chirp parameters closely related to each other:

$$\alpha = a \cdot \frac{\omega_0}{T_p} \frac{1}{(1 + \beta^2)} \quad (3.1.3)$$

$$\beta = \frac{a \cdot \omega_0 \cdot T_p}{4 \cdot \log 2} \quad (3.1.4)$$

where the chirp parameter a represents the relative change in ω_0 within the pulse. As reflected by the expression of $A(t)$ (eq. (3.1.2)) the time dependence of the frequency is indeed linear: $\omega(t) = \omega_0 - \alpha(t - t_{delay})$. Here we note that other forms can be considered as well, but the present study is concerned with the above linear behavior. Our parametrization has the following properties. (i) The time integral of the field is zero (intrinsically fulfilled by real pulses [82]). (ii) The spectrum of the TL and the chirped pulses are the same. (iii) The frequency changing rate ($|\alpha|$) is maximal for the value of $|\beta| = 1$. This maximum is related to the TL pulse duration: $|\alpha|_{max} = 2 \log 2 / T_p^2$. (iv) Finally for small β values ($\beta \ll 1$) the frequency change is proportional to a and ω_0 : $\Delta\omega = \alpha \cdot T_p \approx a \cdot \omega_0$.

The first three of the above features are of great importance in practice, as realistic chirped pulses exhibit the same kind of behavior.

B. The propagation method

For solving the time-dependent nuclear Schrödinger equation (TDSE) of D_2^+ characterized by H_{nuc} in eq. (2.2) one of the most efficient approaches, the multi configuration time-dependent Hartree (MCTDH) method [83–87] has been utilized. This method provides a very efficient algorithm which can determine the quantal motion of the nuclei of a molecular system evolving on one or several coupled electronic potential energy surfaces. It has been applied many times with great success in the last two decades.

For characterizing the vibrational degree of freedom R , we used FFT-DVR (Fast Fourier Transformation-Discrete Variable Representation) with N_R basis elements distributed in the

interval of $R = 0.1 - 80 a.u.$ The rotational degree of freedom θ was described by Legendre polynomials $\{P_J(\cos \theta)\}_{j=0,1,2,\dots,N_\theta}$. These so called primitive basis functions (χ) were utilized to represent the single particle functions (Φ), which in turn were used to expand the total nuclear wave function (ψ):

$$\Phi_{j_s}^{(s)}(s, t) = \sum_{i=1}^{N_s} d_{j_s i}^{(s)}(t) \chi_i^{(s)}(s) \quad s = R, \theta \quad (3.2.1)$$

$$\psi(R, \theta, t) = \sum_{j_R=1}^{n_R} \sum_{j_\theta=1}^{n_\theta} A_{j_R j_\theta}(t) \Phi_{j_R}^{(R)}(R, t) \Phi_{j_\theta}^{(\theta)}(\theta, t) \quad (3.2.2)$$

The actual number of primitive basis functions in the calculations were chosen to be $N_R = 2048$ and $N_\theta = 61$ for the vibrational and rotational degrees of freedom, respectively. On both surfaces and for both coordinates the same number of single particle functions (SPF)s were applied. This number had to be raised as the intensity and pulse length were increasing. Typical values were ranging from $n_R = n_\theta = 10 \dots 20$. Special attention has been payed to the proper choice of basis so that convergence has been reached in each propagation.

IV. RESULTS AND DISCUSSION

Dynamical results eventuating from the numerical wave packet propagations are presented in this section. In our numerical experiment the first pump pulse ionizes the neutral D_2 molecule and generates a nuclear wave packet on the ground electronic state of the molecular ion. A second delayed probe pulse comes then to initiate the dissociation process and leads to fragmentation of the D_2^+ molecular ion. In the probe stage several different laser pulses - covering a wide range of parameters - were used. We especially focus on the effect of the time delay (t_{delay}) and the pulse duration T_p . Above all, the impact of linear frequency chirp constitutes the main subject of this study. All of our results are presented in terms of total dissociation probability.

So as to better understand our dissociation yield results eventuating from linearly chirped laser pulses (see Fig. 2 in [35]), we investigate now short pulse situations ($T_p=1 fs$ and $2 fs$). Using shorter pulses the maximum value of the relative chirp parameter (for $\beta = 1$) corresponds to larger frequency changing rates and, thus the position of the LICI moves faster. If the pulse duration is just a few fs then in our case the position of the LICI can move with approximately the same speed as the wave packet itself. This can help us to study in more detailed the impact of the pulse chirping on observable quantities like the dissociation rate. Moreover, if the pulse duration is much shorter than the period of the field-free vibration of the wave packet, one can probe the time delay dependence of the dissociation probability by getting rid of the effects caused by the averaging over a long period of time and on a wide range of internuclear distances and momenta.

Our results for $T_p=1 fs$ and $2 fs$ are shown in Fig. 2 panels (A) and (C), respectively. Similarly to the situation of longer pulses, the accounted dissociation rates depend strongly upon the delay time t_{delay} . But for short pulses this delay time dependence is not so smooth as has been found for longer pulses (see Fig. 2 in [35]). The curves display definite peaks at certain time delays ca. $8 fs$, $33 fs$ and $57 fs$. Fig. 2 panel (B) shows that at these special delay times during its field-free motion a major portion of the Franck Condon initialized wave packet is crossing the LICI position ($R_{LICI} \sim 2.9 au.$ at $\lambda_0 = 200 nm$) with a positive momentum¹. By inspecting the differences between the negative and positive chirp results

¹ In the presence of the applied laser field the vibrational-rotational wave packet can be considered very

(black dotted lines) it is obvious that the two dissociation curves (dotted red and dashed blue) differ not only at the position of the peaks, but almost in the whole delay time interval. The deviations are significant in the vicinity of the peaks. At the peaks we can notice a significant increased or decreased dissociation rate for negatively or positively chirped pulses, respectively. This finding could be attributed to the fact that for negative chirps the LICI is moving together with the wave packet giving better chance for the dissociation, while in case of positive chirps the opposite effect is observed. However, a little bit away from the dissociation peaks a reverse ordering of the negative and positive chirp dissociation yields is found, namely positively chirped pulses provide larger dissociation rates in those regions (see the negative peaks in the black dotted lines around the positive peaks). The explanation of this finding can be summarized as follows: For delay times that correspond to slightly smaller or larger values than the temporal position of the dissociation peaks, the LICI created by negatively chirped pulses is moving parallel to the wave packet and they avoid each other (no overlap - smaller yield). However, for positive chirps, the LICI is moving in the opposite direction and at the beginning ($t_{delay} > t_{peak}$) or at the end ($t_{delay} < t_{peak}$) of the pulse the position of the LICI and the outgoing wave packet still overlap to some extent giving larger dissociation yield. The impact of the chirp is quite similar for $T_p=2 fs$ (see panel C).

By further increasing the T_p , one encounters a smooth change in the behavior of the dissociation curves. Namely, the characteristic peaks are smoothed out and the delay time dependence is suppressed in the chirped case: the curves become more and more similar to the $T_p = 10 fs$ situation (see Fig. 3 here and Fig. 2 in [35]).

The impact of the chirp is further analyzed in Fig. 4 for $T_p=1 fs$ pulse length. In this figure the dissociation probability is plotted against the chirp parameter a , ranging from $a=-0.3$ to $a=0.3$ ($\beta \approx \mp 1$) at different delay times around one of the peaks ($t_{delay} = 32 \dots 35 fs$). Among the studied delay times the dissociation have the largest rate at $t_{delay} = 33.5 fs$ in the whole inspected parameter range of the chirp. At this special time delay the total dissociation rate depends linearly upon the chirp parameter a . Negative values increase the dissociation rate while the positive chirp suppresses it. Changing the delay time, not only the dissociation rate decreases but more and more pronounced quadratic dependence on the

similar to the field-free one as the small amount of dissociation yield that is provided by using short laser pulse does not modify it significantly. Moreover up to a certain delay time t_{delay*} the two wave packets are completely identical. Minor deviations occur only for $t \gtrsim t_{delay*}$.

chirp parameter can be observed – especially for shorter delay times. As a result of this quadratic dependence, even the negatively chirped pulses provide less dissociation rate than the transform limited one at $t_{delay} = 32 fs$.

The outgoing wave packet has a large amplitude between the 30 fs and 36 fs time delays in which time interval the wave packet of the field-free motion strongly overlaps with the R_{LICI} region. In the above time interval the wave packet is moving outwards, almost reaches its maximal R value and its momentum is decreasing towards 0 but it still remains positive. Therefore, applying a sharp pulse that is centered in the 30 fs -36 fs interval one can achieve relatively significant population transfer since the density is big and at the same time its major part is in the R_{LICI} region.

By chirping the frequency different properties of the pulse can change. Although we preserved the spectra of the pulse and it remained unchanged during the simulations, the effective pulse duration is increased and the effective intensity is decreased by a same factor of $\sqrt{1 + \beta^2}$. As we were interested in using as large frequency changing rate as possible, we have applied pulses with β very close to one, where the widening of the pulses are around $\sqrt{2}$, which - beside the frequency chirping - can also provide a significant effect on the dissociation process. To understand clearly the effect of the pulse widening on the behavior of the dissociation curves obtained for longer pulse durations (see on Fig. 2 in [35]) we performed calculations by using broadened TL pulses and compared the results obtained to the $T_p=10fs$ length chirped ones. Obtained results by this artificially broadened TL pulse ($T_p=14.1 fs$) – despite of the narrower spectra in this case – for the dissociation probabilities were between the original results for $T_p=10 fs$ with positively and negatively chirped pulses. This implies that the suppression of the dissociation yields emerges from the broadening of the chirped pulses and the linearly changing frequency is responsible only for the difference between the dissociation rates belonging to the two kind of chirped pulses.

To check the validity of this explanation for the TL pulses we constructed a model for calculating the dissociation yields for wide pulses with the help of the dissociation yields obtained by using short pulses. In this picture it is assumed that the temporal dissociation rate during the presence of the long pulse is proportional to the temporal intensity and to the calculated total dissociation rate obtained by short pulse. Therefore the dissociation probability with wide pulse (eg. 10 fs) at t_{delay} delay time is obtained by the integrated values of the dissociation probabilities with short pulse (eg. 1 fs) weighted by the envelope

of the given pulse. The respective expression for the approximate dissociation rate can be written as a convolution and reads:

$$P_{diss}^{model}(t_{delay}, T_p^{wide}) = scale * \int_0^\infty P_{diss}(t, T_p^{short}) G(t - t_{delay}) dt \quad (4.1)$$

where $P_{diss}(t, T_p^{short})$ is the dissociation rate for short pulses with $t_{delay} = t$. The convolution function $G(t - t_{delay})$ is the temporal intensity of the Gaussian pulse ,i.e., $G(t - t_{delay}) = e^{-4\log 2 \left(\frac{\Delta t}{T_p^{wide}}\right)^2}$, and the *scale* was chosen to fit the model to real dissociation rate for the situation of wide pulse at a given delay time.

Results of the numerical simulations obtained from the above model are demonstrated in Fig. 5 . After scaling the numerical values obtained from eq. (4.1) so that at a certain point they coincide with the original curve, obtained by the 10 fs pulse calculations, a very good agreement was observed not only for $T_p^{short}=1 fs$, but also for $T_p^{short}=2 fs$ pulses. This agreement perfectly supports our finding, namely that the suppression of the dissociation rate provided by the chirped laser pulses [35], is the effect of the effective pulse widening. When the t_{delay} is in the vicinity of the peaks seen in Fig. 2 then the reduced intensity of the pulse, which is a side effect of the pulse widening, provides a smaller total dissociation yield for the chirped pulse. On the other hand, if the pulse is centered in between two peaks, a wider pulse – despite of the reduced effective intensity – will have a larger temporal intensity at that times when the dissociation can take place with the largest rates.

V. CONCLUSIONS

Linearly varying frequency chirped laser fields of different pulse durations have been applied in the present paper for studying the photodissociation dynamics of D_2^+ . In our treatment the effects of positive, negative and zero chirps have been explored in terms of total dissociation probabilities as a function of delay time between the ionization of D_2 and the maximum of the probe pulse (t_{delay}).

Our study was carried out in the recently introduced LICI framework in which the created light-induced conical intersection is present as long as the laser light is switched on so that the molecule can rotate with respect to the field.

The present paper is a comprehensive study in the sense that besides the effect of chirping, two other laser field parameter dependence, such as T_p and t_{delay} have been investigated.

One of our most important finding is that when the oscillating nuclear wave packet reaches its maximal position along the internuclear coordinate R and its momentum is zero, we were able to fine tune the photodissociation probability. It was demonstrated that when the time delay of the pulse fits to the wave packet being in the above region the use of negatively chirped pulses increases the dissociation probability, while the opposite is true for the positively chirped pulses. Although this observation is not momentous, it is fully consistent with our initial anticipation that the frequency chirping of a pulse results in the movement of the LICI and that this LICI then has a considerable impact on the dynamics.

To continue, we plan to go much beyond and perform calculations using chirped laser pulses in which the time dependence of the laser frequency is designed so as to achieve a desired outcome of a given molecular reaction. Our future prospect is to understand better the relation between the evolving wave packet and the frequency chirping. Being able to directly follow the time evolution of the nuclear wave packet density is expected to open up the possibility to control the dissociation probability or any other dynamical properties of the system under investigation.

Acknowledgments

The authors acknowledge the financial support by the Deutsche Forschungsgemeinschaft (Project ID CE10/50-2). Á.V. also acknowledges the OTKA (NN103251) project. For this

work, the supercomputing service of NIIF has been used.

- [1] M. Born, R. Oppenheimer, *Ann. Phys.* **84**, 457 (1927).
- [2] H. Köppel, W. Domcke, L. S. Cederbaum, *Adv. Chem. Phys.* **57**, 59 (1984).
- [3] M. Baer, *Phys. Rep.* **358**, 75 (2002).
- [4] G. A. Worth, L. S. Cederbaum, *Annu. Rev. Phys. Chem.* **55**, 127 (2004).
- [5] *Conical Intersections: Electronic Structure, Dynamics and Spectroscopy*, edited by W. Domcke, D. R. Yarkony, H. Köppel (World Scientific: Singapore, 2004).
- [6] M. Baer, *Beyond Born Oppenheimer: Electronic Non-Adiabatic Coupling Terms and Conical Intersections* (Wiley: Hoboken, NJ, 2006).
- [7] S. Matsika, *Rev. Comput. Chem.*, **23**, 83 (2007).
- [8] S. C. Althorpe, T. Stecher and F. Bouakline, *J. Chem. Phys.* **129**, 214117 (2008).
- [9] F. Bouakline, *Chem. Phys.* **442**, 31 (2014).
- [10] W. Domcke, D. R. Yarkony, *Annu. Rev. Phys. Chem.* **63**, 325 (2012). (and references therein)
- [11] P. El-Khoury, I. Schapiro, M. Huntress, F. Melaccio, S. Gozem, L. M. Frutos and M. Olivucci, in *CRC Handbook of Organic Photochemistry and Photobiology*. 3rd Edition (eds A. Griesbeck and F. Ghetti) 1029-1056 (CRC Press, Boca Raton, FL, 2012). (and references therein)
- [12] H. H. Fielding, M. A. Robb, *Phys. Chem. Chem. Phys.* **12**, 15569 (2010).
- [13] S. Gozem, A. Krylov and M. Olivucci, *J. Chem. Theo. Comp.* **9**, 284 (2012).
- [14] T. J. Martinez, *Nature* **467**, 412 (2010).
- [15] S. Yamazaki, W. Domcke and A. L. Sobolewski, *J. Phys. Chem. A* **112**, 11965 (2008).
- [16] N. Moiseyev, M. Sindelka and L. S. Cederbaum, *J. Phys. B* **41**, 221001 (2008).
- [17] M. Sindelka, N. Moiseyev and L. S. Cederbaum, *J. Phys. B* **44**, 045603 (2011).
- [18] G. J. Halász, Á. Vibók, M. Sindelka, N. Moiseyev and L. S. Cederbaum, *J. Phys. B* **44**, 175102 (2011).
- [19] G. J. Halász, M. Sindelka, N. Moiseyev, L. S. Cederbaum and Á. Vibók, *J. Phys. Chem. A* **116**, 2636 (2012).
- [20] G. J. Halász, Á. Vibók, M. Sindelka, L. S. Cederbaum and N. Moiseyev, *Chem. Phys.* **399**, 146 (2012).
- [21] G. J. Halász, Á. Vibók, N. Moiseyev and L. S. Cederbaum, *J. Phys. B* **45**, 135101 (2012).

- [22] L. S. Cederbaum, Y. C. Chiang, P. V. Demekhin and N. Moiseyev, *Phys. Rev. Lett.* **106**, 123001 (2011).
- [23] M. Pawlak and N. Moiseyev, *Phys. Rev. A* **92**, 023403 (2015).
- [24] J. Kim, H. Tao, J. L. White, V. S. Petrovi, T. J. Martinez and P. H. Bucksbaum, *J. Phys. Chem. A* **116**, 2758 (2012).
- [25] P. V. Demekhin and L. S. Cederbaum, *J. Chem. Phys.* **139**, 154314 (2013).
- [26] M. Ware, A. Natan, and P. Bucksbaum, Experimental evidence of light induced conical intersection in photodissociation of diatomic molecules, *Bulletin of the American Physical Society* **59**, (2014).
- [27] M. E. Corrales, J. González-Vázquez, G. Balerdi, I. R. Solá, R. de Nalda and L. Bañares, *Nat. Chem.* **6**, 785 (2014).
- [28] A. Natan, M. R. Ware and P. H. Bucksbaum, *Ultrafast Phenomena XIX*, Springer Proceedings in Physics **162**, 122 (2015).
- [29] I. R. Solá, J. González-Vázquez, R. de Nalda, and L. Bañares, *Phys. Chem. Chem. Phys.* **17**, 13183 (2015).
- [30] J. Kim, H. Tao, T. J. Martinez and P. H. Bucksbaum, *J. Phys. B* **48**, 164003 (2015).
- [31] G. J. Halász, Á. Vibók, H. D. Meyer and L. S. Cederbaum, *J. Phys. Chem. A* **117**, 8528 (2013).
- [32] G. J. Halász, Á. Vibók, N. Moiseyev and L. S. Cederbaum, *Phys. Rev. A* **88**, 043413 (2013).
- [33] G. J. Halász, A. Csehi, Á. Vibók and L. S. Cederbaum, *J. Phys. Chem. A* **118**, 11908 (2014).
- [34] G. J. Halász, Á. Vibók and L. S. Cederbaum, *J. Phys. Chem. Lett.* **6**, 348 (2015).
- [35] A. Csehi, G. J. Halász, L. S. Cederbaum and Á. Vibók, *J. Chem. Phys.* **143**, 014305 (2015).
- [36] G. J. Halász, A. Csehi and Á. Vibók, *Theor. Chem. Acc.* **134**, 128 (2015).
- [37] A. D. Bandrauk and M. Sink, *Chem. Phys. Lett.* **57**, 569 (1978).
- [38] A. D. Bandrauk and M. Sink, *J. Chem. Phys.* **74**, 1110 (1981).
- [39] A. Zavriyev, P. H. Bucksbaum, H. G. Muller and D. V. Schumacher, *Phys. Rev. A* **42**, 5500 (1990).
- [40] E. E. Aubanel, J. M. Gauthier and A. D. Bandrauk, *Phys. Rev. A* **48**, 2145 (1993).
- [41] E. Charron, A. Giusti-Suzor and F. H. Mies, *Phys. Rev. A* **49**, R641 (1994).
- [42] S. Chelkowski, T. Zuo, O. Atabek and A. D. Bandrauk, *Phys. Rev. A* **52**, 2977 (1995).
- [43] A. Giusti-Suzor, F. H. Mies, L. F. DiMauro, E. Charron and B. Yang, *J. Phys. B* **28**, 309 (1995).

- [44] R. Numico, A. Keller and O. Atabek, Phys. Rev. A **52**, 1298 (1995).
- [45] I. Sánchez and F. Martín, Phys. Rev. A **57**, 1006 (1998).
- [46] K. Sandig, H. Figger and T. V. Hansch, Phys. Rev. Lett. **85**, 4876 (2000).
- [47] V. N. Serov, A. Keller, O. Atabek and N. Billy, Phys. Rev. A **68**, 053401-1 (2003).
- [48] J. H. Posthumus, Rep. Prog. Phys. **67**, 623 (2004).
- [49] V. N. Serov, A. Keller, O. Atabek, H. Figger and D. Pavidic, Phys. Rev. A **72**, 033413 (2005).
- [50] M. Uhlmann, T. Kunert and R. Schmidt, Phys. Rev. A **72**, 045402-1 (2005).
- [51] P. Q. Wang, A. M. Sayler, K. D. Carnes, J. F. Xia, M. A. Smith, B. D. Esry and I. Ben-Itzhak, Phys. Rev. A **74**, 043411-1 (2006).
- [52] F. Anis and B. D. Esry, Phys. Rev. A **77**, 033416-1 (2008).
- [53] F. Anis, T. Cackowski, B. D. Esry, J. Phys. B **42**, 091001-1 (2009).
- [54] J. J. Hua and B. D. Esry, Phys. Rev. A **80**, 013413 (2009).
- [55] S. Adhikari, A. K. Paul, D. Mukhopadhyay, G. J. Halász, Á. Vibók, R. Baer and M. Baer, J. Phys. Chem. A **113**, 7331 (2009).
- [56] A. K. Paul, S. Adhikari, M. Baer and R. Baer, Phys. Rev. A **81**, 013412-1 (2010).
- [57] C. R. Calvert, W. A. Bryan, W. R. Newell and I. D. Williams, Phys. Rep. **491**, 1 (2010).
- [58] U. Thumm, T. Niederhausen and B. Feuerstein, Phys. Rev. A **77**, 063401-1 (2008).
- [59] M. Fischer, F. Grossmann, R. Schmidt, J. Handt, S. M. Krause and J. M. Rost, New. J. Phys. **13**, 053019-1 (2011).
- [60] M. Fischer, U. Lorenz, B. Schmidt and R. Schmidt, Phys. Rev. A **84**, 033422-1 (2011).
- [61] J. McKenna, F. Anis, A. M. Sayler, B. Gaire, N. G. Johnson, E. Parke, K. D. Carnes, B. D. Esry and I. Ben-Itzhak, Phys. Rev. A **85**, 023405-1 (2012).
- [62] H. X. He, R. F. Lu, P. Y. Zhang, K. L. Han and G. Z. He, J. Chem. Phys. **136**, 024311-1 (2012).
- [63] Y. Furukawa, Y. Nabekawa et al., Opt. Lett. **37**, 2922 (2012).
- [64] J. Handt, S. M. Krause, J. M. Rost, M. Fischer, F. Grossmann and R. Schmidt, arXiv 2011, arXiv:1103.1565v2.
- [65] A. Igarashi, Eur. Phys. J. D, **68**, 266 (2014).
- [66] D. J. Haxton, Phys. Rev. A **88**, 013415 (2013).
- [67] D. J. Haxton, K. V. Lawler and C. W. McCurdy, Phys. Rev. A **91**, 062502 (2015).
- [68] V.S. Malinovsky and J.L. Krause, Eur. Phys. J. D **14**, 147 (2001).

- [69] A. Datta, S. S. Bhattacharyya and B. Kim, *Phys. Rev. A* **65**, 043404 (2002).
- [70] G. Katz, M. A. Ratner and R. Kosloff, *New J. Phys.* **12**, 015003 (2010).
- [71] V. S. Prabhudesai, U. Lev, A. Natan, B. D. Bruner, A. Diner, O. Heber, D. Strasser, D. Schwalm, I. Ben-Itzhak, J. J. Hua, B. D. Esry, Y. Silberberg, D. Zajfman, *Phys. Rev. A* **81**, 023401 (2010).
- [72] A. Natan, U. Lev, V. S. Prabhudesai, B. D. Bruner, D. Strasser, D. Schwalm, I. Ben-Itzhak, O. Heber, D. Zajfman and Y. Silberberg, *Phys. Rev. A* **86**, 043418 (2012).
- [73] V. S. Prabhudesai, A. Natan, B. D. Bruner, Y. Silberberg, U. Lev, O. Heber, D. Strasser, D. Schwalm, D. Zajfman, I. Ben-Itzhak, *J. Kor. Phys. Soc.* **59**, 2890 (2011).
- [74] B. Y. Chang, S. Shin, J. Santamaria and I. R. Sola, *J. Phys. Chem. A* **116**, 2691 (2012).
- [75] S. Askeland and M. Førre, *Phys. Rev. A* **88**, 043411 (2013).
- [76] C. P. Zhang, X. Y. Miao, *Spect. Lett.* **47**, 267 (2014).
- [77] U. Lev, L. Graham, C. B. Madsen, I. Ben-Itzhak, B. D. Bruner, B. D. Esry, H. Frosting, O. Heber, A. Natan and V. S. Prabhudesai, *J. Phys. B* **48**, 201001 (2015).
- [78] D. V. Novitsky, *Optic Comm.* **358**, 202 (2016).
- [79] F. V. Bunkin and I. I. Tugov, *Phys. Rev. A* **8**, 601 (1973).
- [80] S. I. Chu, C. Laughlin, and K. Datta, *Chem. Phys. Lett.* **98**, 476 (1983).
- [81] S. I. Chu, *J. Chem. Phys.* **75**, 2215 (1981).
- [82] D. B. Milosevic, G. G. Paulus, D. Bauer, and W. Becker, *J. Phys. B* **39**, R203 (2006).
- [83] H. D. Meyer, U. Manthe and L. S. Cederbaum, *Chem. Phys. Lett.* **165**, 73 (1990).
- [84] U. Manthe, H. D. Meyer and L. S. Cederbaum, *J. Chem. Phys.* **97**, 3199 (1992).
- [85] M. H. Beck, A. Jäckle, G. A. Worth and H. D. Meyer, *Phys. Rep.* **324**, 1 (2000).
- [86] G. A. Worth et al. The MCTDH package, version 8.2; University of Heidelberg: Heidelberg, Germany, 2000. H. D. Meyer et al. The MCTDH package, versions 8.3 and 8.4; University of Heidelberg, Germany, 2002 and 2007. <http://mctdh.uni-hd.de/>.
- [87] *Multidimensional Quantum Dynamics: MCTDH Theory and Applications*, edited by H. D. Meyer, F. Gatti, G. A. Worth, (Wiley-VCH: Weinheim, 2009).

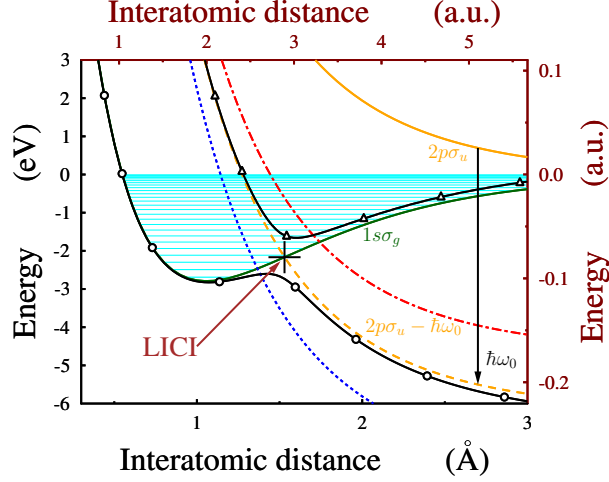


Figure 1: Potential energy curves of the D_2^+ molecular ion. Diabatic energies of the ground $1s\sigma_g$ and the first excited $2p\sigma_u$ states are displayed with solid green and orange lines, respectively. The field dressed excited states ($2p\sigma_u - \omega_0$) are presented for three different chirp situations (transform limited, dashed orange line; positively chirped, dotted blue line; negatively chirped, dashed-dotted red line). These field dressed excited states ($2p\sigma_u - \omega_0$) form light-induced conical intersections (LICIs) with the ground state. Only for the case of a transform limited laser frequency $\omega_0 = 6.199 \text{ eV}$ and field intensity of $3 \times 10^{13} \frac{W}{cm^2}$, a cut through the adiabatic surfaces at $\theta = 0$ (parallel to the field) is also shown by solid black lines marked with circles (V_l) and triangles (V_u). For the transform limited case, we denote with a cross the position of the LICl ($R_{LICl} = 1.53 \text{ \AA} = 2.891 a.u.$ and $E_{LICl} = -2.16611 eV$).

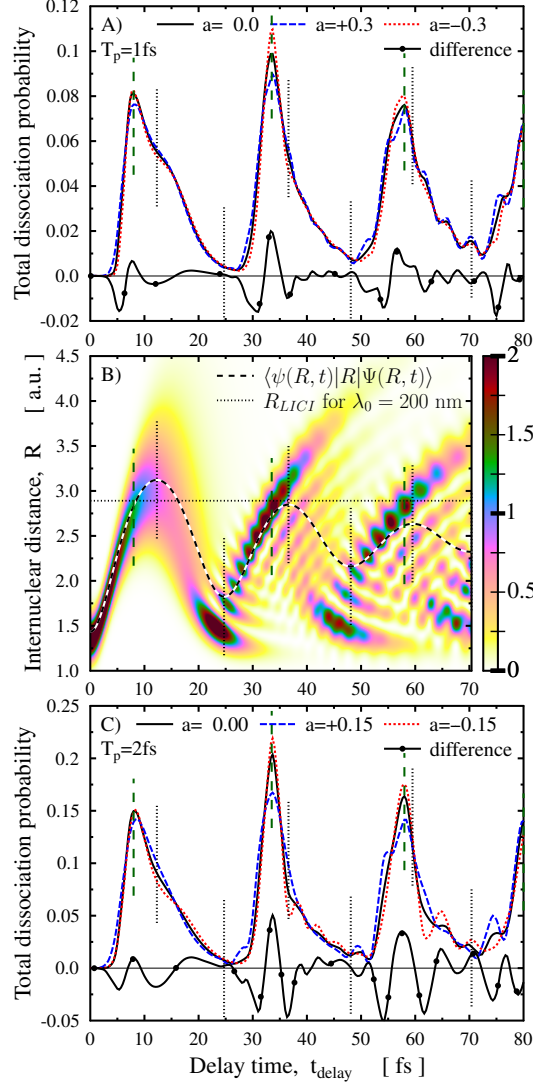


Figure 2: Dissociation probabilities of D_2^+ as a function of the delay time t_{delay} of the probe pulse. The peak intensity is $10^{13}W/cm^2$ and the central wavelength is $200nm$. All the panels include positive, negative and TL chirp cases with the pulse duration being $1fs$ and $2fs$ (panels (A) and (C), respectively). In these panels the black dotted curves present the difference between the dissociation probabilities obtained by the positively and negatively chirped pulses. Panel (B) shows the field-free vibration of the system. Here the square of the vibrational wave function is represented by color code: the darker the color the larger the amplitude of the wave packet. The vertical dashed green and dotted black lines represent the position of the local maxima of the dissociation probabilities obtained by $1fs$ pulse and the extremal positions of the average internuclear distances, respectively.

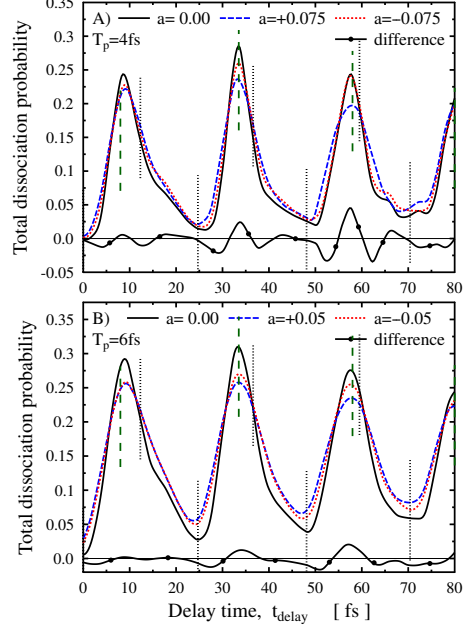


Figure 3: Dissociation probabilities of D_2^+ as a function of the delay time t_{delay} of the probe pulse. The peak intensity is 10^{13} W/cm^2 and the central wavelength is 200 nm . Both panels include positive, negative and TL chirp cases with the pulse duration being 4 fs and 6 fs (panels (A) and (B), respectively). The chirp parameters were $a = \pm 0.075$ and $a = \pm 0.05$ for the 4 fs and 6 fs pulses, respectively. The black dotted curves present the difference between the dissociation probabilities obtained by the positively and negatively chirped pulses. The vertical dashed green and dotted black lines represent the position of the local maxima of the dissociation probabilities obtained by 1 fs pulse and the extremal positions of the average internuclear distances, respectively.

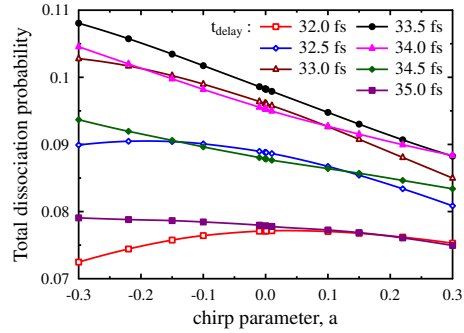


Figure 4: Dissociation probabilities of D_2^+ as a function of the chirp parameter around $t_{\text{delay}} = 33.5 \text{ fs}$ for a peak intensity of 10^{13} W/cm^2 . The central wavelength is 200 nm and $T_p = 1 \text{ fs}$.

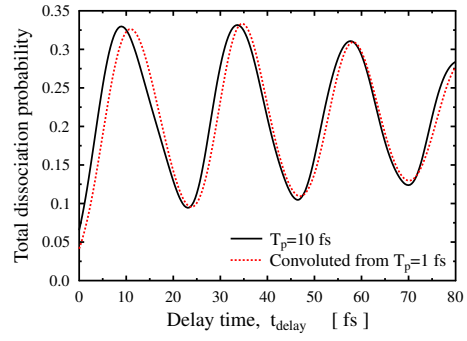


Figure 5: Comparison of dissociation probabilities for D_2^+ . Black line: results of wave packet propagation ($T_p = 10 \text{ fs}$); red line: values calculated according to eq. (4.1) obtained by weighting the $T_p = 1 \text{ fs}$ probabilities.